JMEPEG (2017) 26:1598–1604
DOI: 10.1007/s11665-017-2588-8

1059-9495/$19.00

Structure and Electrical Properties of Mn-Cu-O Spinels

M. Bobruk, K. Durczak, J. Dąbek, and T. Brylewski

(Submitted October 5, 2016; in revised form February 1, 2017; published online March 13, 2017)

The study presents the results of structural and electrical conductivity investigations of a $Cu_{1.3}Mn_{1.7}O_4$ spinel obtained using EDTA gel processes. An amorphous gel was synthesized and calcinated for 5 h in air at temperatures of 673, 773, 873, and 973 K. When calcinating the gel at temperatures below 973 K, the obtained powders consisted of two phases—the regular $Cu_{1.5}Mn_{1.5}O_4$ spinel and manganese(III) oxide. At 973 K, Mn_2O_3 was no longer observed, but a new Mn_3O_4 phase appeared in addition to the $Cu_{1.5}Mn_{1.5}O_4$ spinel. Green bodies prepared from these powders were sintered for 2 h in air at 1393 K. The obtained sinters had a porosity of around 12% and were composed predominantly of the spinel phase, with minor amounts of Mn_3O_4 and, in the case of three of four sinters—CuO. Electrical conductivity measurements were taken over the temperature range of 300-1073 K. A change in the character of conductivity of the studied sinters was observed in the range of 400-430 K, and it was associated with an increase in activation energy from 0.20 to 0.56 eV. The electrical conductivity of the studied sinters ranged from 74.8 to 88.4 S cm^{-1}, which makes the $Cu_{1.3}Mn_{1.7}O_4$ material suitable for application as a protective-conducting coating in IT-SOFC ferritic stainless steel interconnects.

Keywords electrical conductivity, solid oxide fuel cell (SOFC), spinel solid solutions, x-ray

1. Introduction

Ceramic materials with a composition expressed by the general formula AB_2X_4, where A and B are metal cations, and X is a divalent anion, are interesting because of their unique physicochemical properties. In a spinel with a regular structure, cations can occupy either the tetragonal positions (A)—in the case of divalent ions, or the octahedral position (B)—in the case of tri- and quadrivalent ions (Ref 1, 2). Spinels exhibit a wide range of electrical properties; some of them are insulators, and some of them have a metallic character. These properties strongly depend on the type of ion and its position in the unit cell (Ref 3). Ions that occupy octahedral positions are responsible for characteristics related to electrical conductivity (Ref 3). Different valence states of octahedral cations are thus beneficial for conduction (Ref 2). In this respect, the application of manganese as a component of a spinel which is to exhibit electrical conductivity at high temperatures is well-justified due to the multiple valence states of manganese ions.

In recent years, manganese-copper spinels have been the subject of intensive research activities due to their wide application in heterogeneous catalysis. The $Cu_{1.3}Mn_{1.7}O_4$ spinel, which exhibits the very high electrical conductivity of 225 S cm^{-1} at 1023 K (Ref 2), appears to be a particularly suitable candidate as a protective-conducting material for the surface modification of interconnects based on ferritic stainless steels and used in intermediate-temperature solid oxide fuel cells (IT-SOFCs) (Ref 4-14).

It is not easy to synthesize this spinel with the nominal composition due to the narrow range in which the regular phase is observed, i.e., $0.75 \leq x \leq 1.15$ for $Cu_xMn_{3-x}O_4$, according to the phase diagram of the CuO-MnO_2 system at 1073 K (Ref 15). Since the range of composition of the spinel in question and, subsequently, its structural and electrical properties are strongly dependent on the method of its synthesis, attempts have been made to synthesize a single-phase spinel using numerous wet chemistry methods. One of the methods which seem promising is the modified sol-gel method utilizing EDTA as a complexing agent of metal cations in a water solution, also known as the EDTA gel processes (Ref 16, 17). The idea of the EDTA gel processes applied in the present work, i.e., one based on water-soluble metal chelates, is to reduce the concentration of free metal ions in the precursor solution through the formation of strong, soluble chelate complexes which are then converted into an amorphous glassy state when the solvent is removed (Ref 18). This method is especially useful in this case due to the high conditional stability constant of complexes of EDTA anions with Cu and Mn ions (Ref 19).

The aim of the present paper was to synthesize an amorphous gel precursor via the EDTA gel processes and to thoroughly investigate the structure and electrical properties of the $Cu_{1.3}Mn_{1.7}O_4$ powders and sinters.

2. Experimental

The $Cu_{1.3}Mn_{1.7}O_4$ spinel was synthesized by thermally decomposing a gel precursor with the use of the EDTA gel processes (Ref 17). Analytical grade manganese nitrate (Mn $(NO_3)_2 \cdot 4H_2O$, Sigma Aldrich) and copper nitrate (Cu

M. Bobruk, J. Dąbek, and T. Brylewski, Faculty of Materials Science and Ceramics, AGH University of Science and Technology, al. Mickiewicza 30, 30-059 Kraków, Poland; and **K. Durczak**, Faculty of Agronomy and Bioengineering, Institute of Biosystems Engineering, Poznań University of Life Sciences, ul. Wojska Polskiego 50, 60-627 Poznan, Poland. Contact e-mail: brylew@agh.edu.pl.

$(NO_3)_2 \cdot 2.5H_2O$, Sigma-Aldrich) starting solutions with known concentrations were mixed in a molar ratio corresponding to the nominal stoichiometric composition of $Cu_{1.3}Mn_{1.7}O_4$. A 0.1 M $(NH_4)_4$EDTA (Sigma-Aldrich, analytical grade) solution was then added to the mixture prepared as specified above at a molar ratio of 1:1.1. In addition, drops of ammonium hydroxide were added until the solution had a pH of 8. The obtained mixture was then heated until an amorphous gel was obtained; the gel was then dried. By pyrolyzing and calcinating the gel for 5 h in air at 673, 773, 873, and 973 K, four types of powders were obtained and then milled. The powders were first compacted at a pressure of 40 MPa, and then cold-pressed isostatically at a pressure of 250 MPa. The green bodies obtained in this way were sintered for 2 h in air at 1393 K.

The phase compositions of both the powders and the sinters were carried out by means of x-ray diffraction (XRD), using the X'Pert Pro PW 3710 diffractometer manufactured by PANalytical. Qualitative phase analyses were performed based on the Rietveld profile refinement method, using HighScore Plus software (PANalytical) coupled with the X`Pert diffractometer and the standard PCPDFWIN v.2.3 data set. The Scherrer dependence, given in (Ref 20), was used to estimate the size of crystallites of the investigated powders.

Morphological observations and chemical composition analyses of the powders were performed by means of the FEI Nova NanoSEM 200 scanning electron microscope equipped with an energy-dispersive x-ray spectrometer (EDS).

The density of the sinters was determined based on the known values of true density—established by means of a helium pycnometer (AccuPyc HP 1340), apparent density—measured by means of the Archimedes method, using water as the immersion medium, and theoretical density—calculated based on crystallographic data. The relative density of the samples was determined by dividing the apparent density by the theoretical density. The open and total porosities were computed using the following equations:

$$P_o = \frac{V_o - V_{pic}}{V_o} \cdot 100\% \quad \text{(Eq 1)}$$

$$P_c = \left(1 - \frac{d_a}{d_{XRD}}\right) \cdot 100\% \quad \text{(Eq 2)}$$

where: P_o—open porosity (%), P_c—total porosity (%), V_o—geometric volume (cm^3), V_{pic}—volume determined using the pycnometer (cm^3), d_a—apparent density (g cm^{-3}), and d_{XRD}—theoretical density (g cm^{-3}).

The electrical resistance of the examined sinters was measured using two different methods. For the temperature range of 300-673 K, electrochemical impedance spectroscopy (EIS) was applied; the device used in this case was the Autolab PGSTAT302N, with a frequency range of 10^6-10^{-1} Hz and an amplitude of 350 mV. For measurements in the range of 673-1073 K, the four-point, two-probe dc method was utilized, with a current intensity of 0.01 A, using the ZS-2002 programmable power supply manufactured by JOTA (Poland).

3. Results and Discussion

Figure 1 presents the diffraction patterns of powders with the nominal composition of $Cu_{1.3}Mn_{1.7}O_4$ obtained after 5 h of calcination of gel in air at temperatures from 673 to 973 K. An ex situ XRD phase analysis of these powders obtained after the thermal treatment of the gel at temperatures below 973 K revealed that these samples contain two phases—the $Cu_{1.5}Mn_{1.5}O_4$ spinel with a regular structure (ICDD 01-070-0262) and manganese(III) oxide (ICDD 01-10-0069). In the case of the gel calcinated at 973 K, the Mn_2O_3 phase was no longer observed; it was replaced by Mn_3O_4 (ICDD 01-4-0732). The value of lattice parameter a of the unit cell of the manganese-copper spinel in the investigated powders did not vary significantly, ranging from 8.2860 to 8.2900 Å.

As the temperature of gel calcination increased, so did the size of the crystallites of the main spinel phase, which grew from 32 to 70 nm. Combustion synthesis is what makes it possible to achieve grains with such a small size (Ref 21). The SEM micrographs of powders with the nominal composition of $Cu_{1.3}Mn_{1.7}O_4$ obtained after calcinating gel for 5 h in air at temperatures from 673 to 973 K show their fine-crystalline nature (Fig. 2). It should be emphasized that the investigated powders were not milled, but merely sifted through a sieve. Based on these observations it was determined that the grains of the powders were approximately oval in shape, and that they tended to form agglomerates consisting of numerous grains. The size of the grains increased together with calcination temperature and ranged from 180 to 300 nm.

Ex situ XRD observations of the sinters obtained by thermally treating green bodies (which were themselves based on powders calcinated at 673, 773, 873, and 973 K) for 2 h in air at 1393 K revealed the presence of the spinel phase and a certain amount of Mn_3O_4 and CuO phases. Figure 3 shows the diffraction patterns obtained for these sinters.

Table 1 lists the results of the relative mass contribution of phases formed after subjecting sinters based on powders calcinated at 673, 773, 873, and 973 K to 2 h of thermal treatment in air at 1393 K; the actual compositions of the spinels calculated based on these data are also listed. These results indicate that all studied sinters contained spinel as the predominant phase and a small amount of Mn_3O_4. In all sinters except for the one based on the powder calcinated at 673 K, copper(II) dioxide was found; the highest contribution of this compound was observed for the sinter obtained from the powder calcinated at 773 K. The determined compositions of the spinels did not differ significantly from the nominal composition, i.e., $Cu_{1.3}Mn_{1.7}O_4$.

The density of the $Cu_{1.3}Mn_{1.7}O_4$ sinters was determined from known values of true density established by means of a helium pycnometer, apparent density and theoretical density calculated based on crystallographic data. The open porosity of all investigated sinters was very low—at the level of around 0.1%—and was thus neglected when calculating total porosity. Table 2 lists the values of total porosity as well as the theoretical and relative densities of the investigated samples after 2 h of sintering in air at 1398 K. The data presented in this table show that all studied samples exhibited similar porosity (ca. 12%) and a density of approximately 88% of theoretical density.

Figure 4 shows the SEM micrographs of the fracture cross sections of the sinters obtained by sintering the green bodies (which were themselves based on powders calcinated at 673, 773, 873, and 973 K) for 2 h in air at 1393 K. The morphology of the individual samples did not differ significantly. The sinters

consisted of coarse grains with a regular structure, with inter-agglomerate pores of considerable size interspersed between them. The size of these grains ranged from 6 to 15 μm.

The electrical conductivity of the sinters obtained in the study was measured using two methods. The two-probe ac technique combined with electrochemical impedance

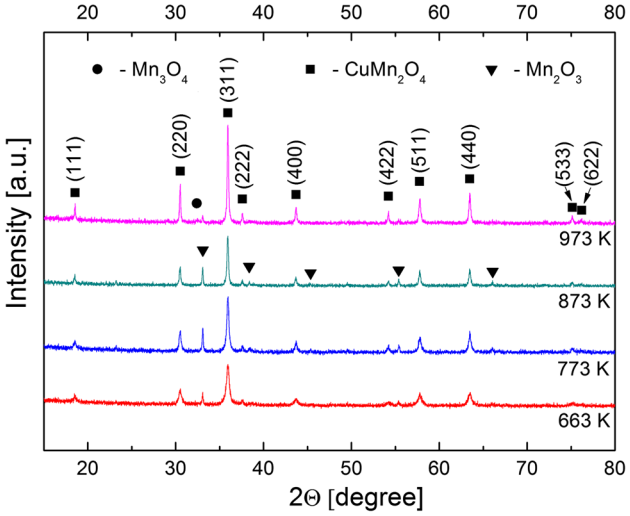

Fig. 1 Diffraction patterns of powders with the nominal composition of $Cu_{1.3}Mn_{1.7}O_4$ obtained after the calcination of gel at different temperatures

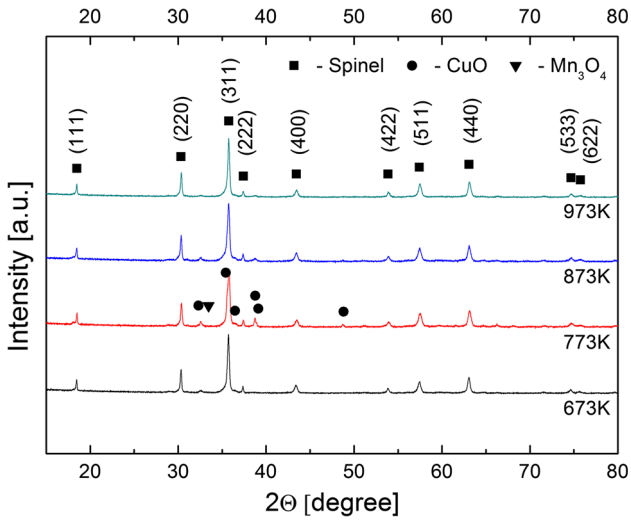

Fig. 3 Diffraction patterns of sinters based on powders with the nominal composition of $Cu_{1.3}Mn_{1.7}O_4$ obtained after the calcination of gel at different temperatures

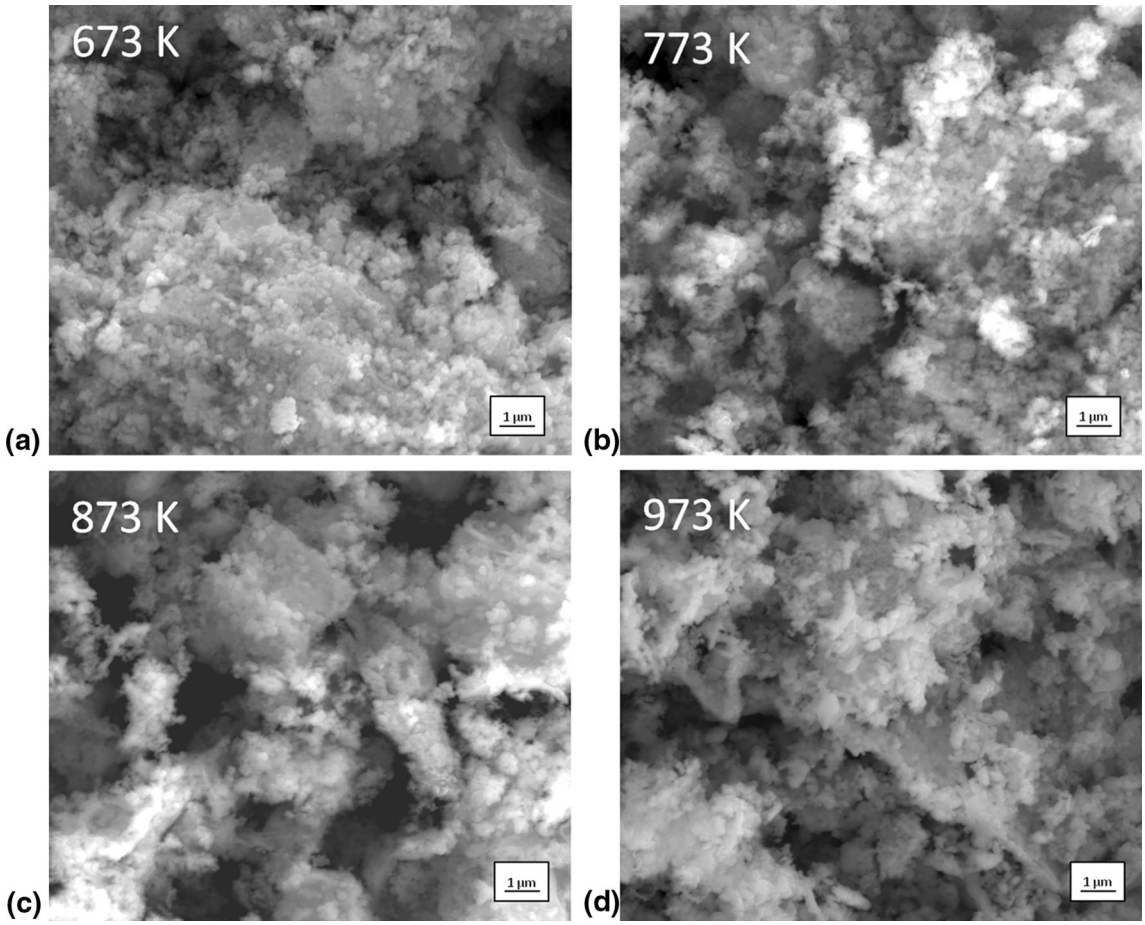

Fig. 2 SEM micrographs of powders with the nominal composition of $Cu_{1.3}Mn_{1.7}O_4$ obtained after the calcination of gel at different temperatures

Table 1 Relative mass contribution of phases identified in sinters and the corresponding actual spinel compositions

Gel calcination temperature, K	Mass contribution, %			Actual composition of spinel
	Spinel	Mn_3O_4	CuO	
673	95.4	4.6	…	$Cu_{1.36}Mn_{1.64}O_4$
773	84.0	5.3	10.7	$Cu_{1.31}Mn_{1.69}O_4$
873	90.0	5.0	5.0	$Cu_{1.34}Mn_{1.66}O_4$
973	94.7	2.4	2.9	$Cu_{1.32}Mn_{1.68}O_4$

Table 2 Total porosity and theoretical and relative densities of the studied sinters after 2 h of sintering in air at 1393 K

Gel calcination temperature, K	Total porosity, %	Theoretical density, g/cm^3	Relative density, %
673	11.6	5.4338	88.4
773	12.4	5.4528	87.6
873	11.7	5.4451	88.3
973	11.6	5.4485	88.4

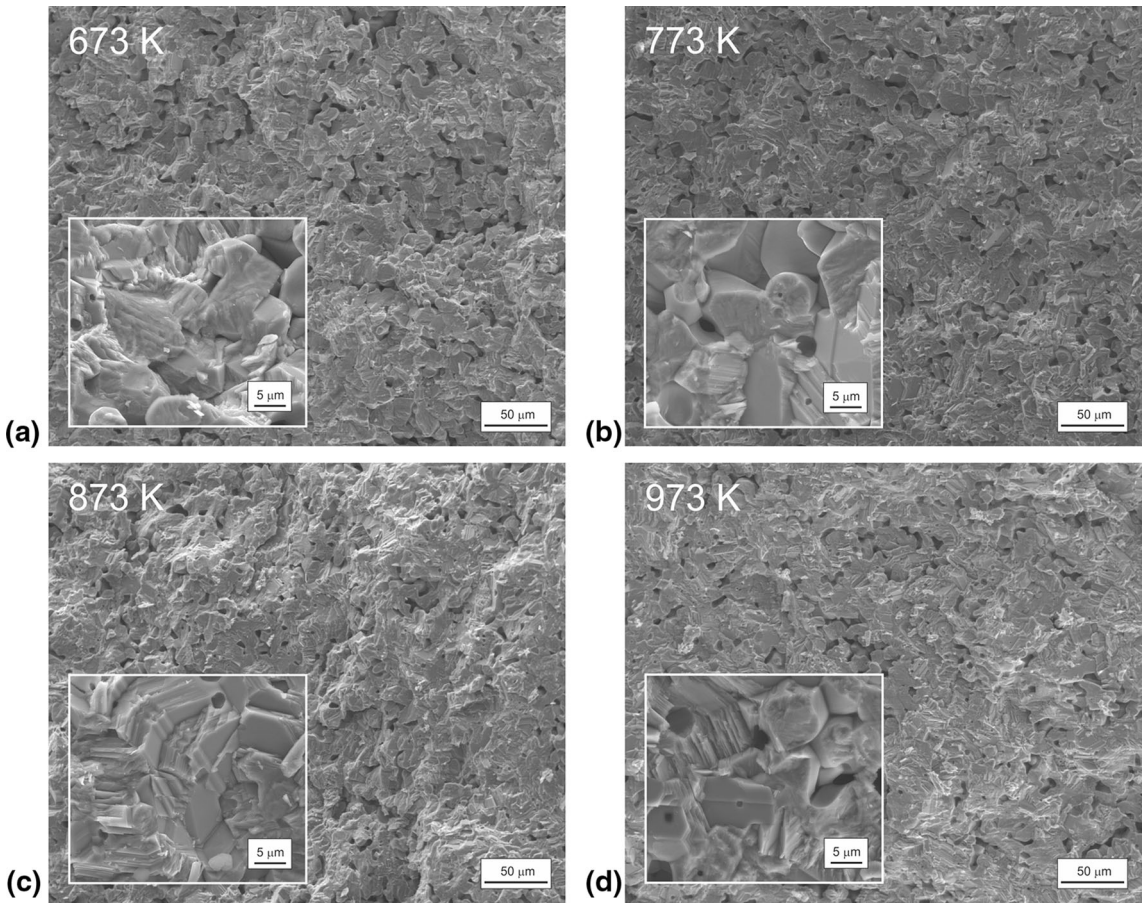

Fig. 4 SEM micrographs of fracture cross sections of sinters with the nominal composition of $Cu_{1.3}Mn_{1.7}O_4$ obtained for different temperatures of gel calcination

spectroscopy (EIS) was used in the temperature range of 300-673 K, while the four-point, two-probe dc method was applied in the range of 673-1073 K. Equivalent circuits were fit based on sets of measurement points from impedance spectra. In the case of the conductivity measurements taken in the range of 348-473 K, a single impedance semi-circle was observed, which is why the equivalent circuit determined via fitting consisted of a resistor and a CPE element connected in parallel; in the case of polycrystalline samples, the CPE element is often observed instead of a Debye capacitor due to the heterogeneous and porous character of the material (Fig. 5a). On the other hand, the data obtained during measurements at 498-673 K indicate the presence of semicircles with a negative part of imaginary impedance; these semicircles converge to zero with

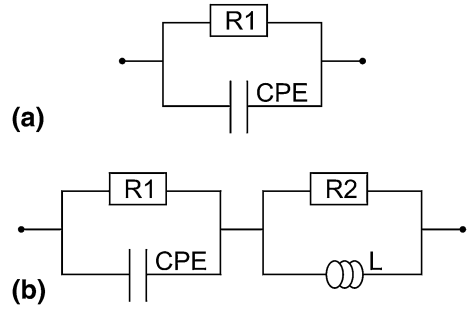

Fig. 5 Equivalent circuits used to model impedance spectra

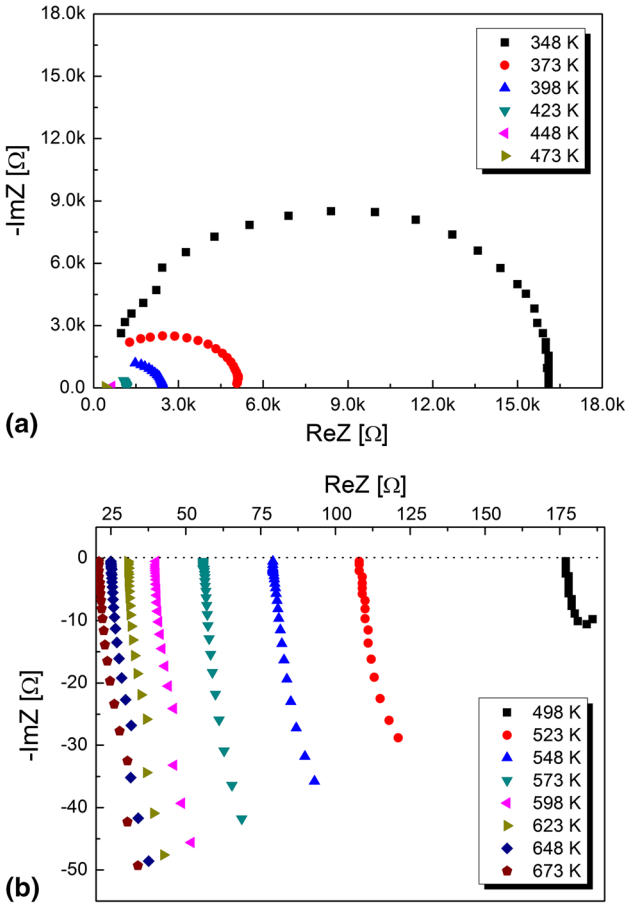

Fig. 6 Impedance spectra for the sinter based on the powder obtained after calcinating gel at 673 K, recorded in the following temperature ranges: (a) 348-473 K and (b) 498-673 K

the decrease in frequency. In this case, the equivalent circuit also needs to include an induction coil, as shown in Fig. 5(b).

Figure 6 shows examples of Nyquist impedance plots for sinters based on the powder obtained after calcinating gel at 673 K; these plots were recorded when performing measurements in two temperature ranges, i.e., 348-473 K (Fig. 6a) and 498-673 K (Fig. 6b). The electrical resistance values obtained from the equivalent circuits and the geometrical dimensions of the samples were used to determine their conductivity based on the following dependence:

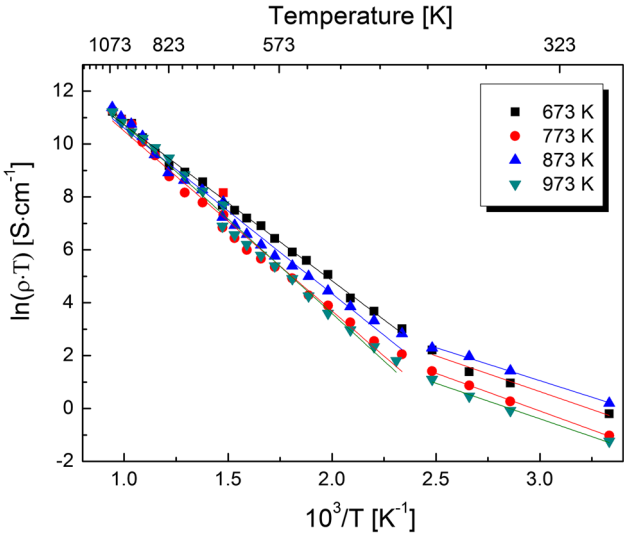

Fig. 7 Temperature dependence of electrical conductivity of sinters based on powders calcinated at temperatures of 673, 773, 873, and 973 K in an Arrhenius plot

$$\sigma = \frac{h}{R \cdot A} \qquad \text{(Eq 3)}$$

where: R—electrical resistance (Ω), A—cross-sectional surface area (cm^2), h—sample thickness (cm).

Figure 7 shows the temperature dependence of the electrical conductivity of the studied sinters in an Arrhenius plot. It is clear from the plot that the electrical conductivity of all samples increases together with temperature, which confirms their semiconductor nature.

Literature data (Ref 21, 22) suggest that electrical conduction in manganese spinels occurs as a result of electrons hopping between Mn^{3+} and Mn^{4+} ions, which have a strong tendency to occupy octahedral sites. Electron hopping between manganese ions in octahedral positions is also presumed in the $Cu_xMn_{3-x}O_4$ spinel ($0 \le x \le 0.2$). In this case, the conduction mechanism entails the exchange of electrons between ions that are present in the crystal lattice in various oxidation states. In the presence of copper ions, the electron hopping may proceed according to the following equation (Ref 23):

$$Cu^{2+} + Mn^{3+} \Leftrightarrow Cu^{+} + Mn^{4+} \qquad \text{(Eq 4)}$$

The addition of copper thus favors an increase in the concentration of Mn^{4+} ions that participate in the process of electrical conduction in the manganese-copper spinel.

A change in the inclination of the curves representing the discussed dependence ($\ln(\sigma \cdot T) = f(1/T)$) can also be observed in Fig. 7 in the range of 400-430 K. The highest conductivity in the range of 300-400 K was observed for the sinter based on the powder obtained after the calcination of gel at 873 K. When the measurements were taken in the range from 430 to 770 K, the highest electrical conductivity was observed for the sinter based on the powder prepared as a result of calcination at 673 K. In the case of both of these ranges, the least desirable electrical properties were measured for the sinter based on the powder obtained at the calcination temperature of 973 K. The changes that are observed over the temperature range of 770-1073 K are

Table 3 Activation energy of electrical conduction (E_a), electrical conductivity (σ_m) measured at 1073 K, and electrical conductivity (σ_d) after adjusting for porosity, as observed for sinters with the nominal composition of $Cu_{1.3}Mn_{1.7}O_4$ depending on the temperature of gel calcination

Gel calcination temperature, K	E_a, eV		σ_m (1073 K), S cm^{-1} (measured)	σ_d (1073 K), S cm^{-1} (calculated from Eq 6)
	$T \leq 400$ K	$T \geq 430$ K		
673	0.20 ± 0.02	0.45 ± 0.01	76.1	91.1
773	0.22 ± 0.01	0.53 ± 0.01	78.5	95.1
873	0.19 ± 0.01	0.48 ± 0.01	88.4	105.8
973	0.20 ± 0.01	0.56 ± 0.01	74.8	89.5

slight. Increasing the temperature of the samples favors the increased vibrations of the crystal lattice and, subsequently, the reduction in the distance between the ions. As a result, the probability of electron hopping between pairs of Mn^{3+}/Mn^{4+} and Cu^{+}/Cu^{2+} ions occupying octahedral sites grows.

The linear course of the $\ln(\sigma \cdot T) = f(1/T)$ dependence observed for two temperature ranges, i.e., below 400 K and above 430 K indicate the thermally activated character of the electrical conductivity of the studied sinters (Fig. 7), in accordance with the Nernst-Einstein dependence:

$$\ln(\sigma_m \cdot T) = \ln \sigma_o - \frac{E_a}{k \cdot T} \quad \text{(Eq 5)}$$

where: σ_m—electrical conductivity (Ω^{-1} cm^{-1}), σ_o—pre-exponential factor (Ω^{-1} cm^{-1} K^{-1}), E_a—activation energy of electrical conduction (eV), k—Boltzmann's constant (eV K^{-1}), T—temperature (K).

The activation energy of electrical conduction of the studied samples was calculated based on the linear dependences shown in Fig. 7. The results of these calculations for two temperature ranges, i.e., $T \leq 400$ K and $T \geq 430$ K, are shown in Table 3, which also shows the values of electrical conductivity (σ_m) measured at 1073 K and electrical conductivity adjusted for porosity (σ_d). The latter values were obtained by applying the effective medium theory (Ref 24):

$$\sigma_d = \sigma_m \cdot \frac{2 + p}{2 - 2p} \quad \text{(Eq 6)}$$

where: p—fraction of total porosity, σ_d—electrical conductivity of a dense sinter (S cm^{-1}) and σ_m—electrical conductivity of a porous sinter (S cm^{-1}). Based on dependence (6), the bulk properties of the sample were established; the contribution of surface conduction processes was determined to be minimal and, as such, it was neglected.

Based on these results, it can be concluded that activation energies of electrical conduction of manganese-copper spinels at temperatures below 400 K are lower and at a comparable level, which indicates that the temperature of gel calcination has no influence, while above 430 K higher activation energies are observed. This can suggest the possible change in the mechanism of conduction in the investigated sinters. Such a change can occur due to an increase in the amount of charge carriers in the transport within the grains, whereas in the lower temperature range, the predominant mechanism is conduction via grain boundaries. This phenomenon shall be investigated further. It should be emphasized that the determined activation energies for $Cu_{1.3}Mn_{1.7}O_4$ sinters are lower than those observed for $Cu_xMn_{3-x}O_4$ ($0.9 \leq x \leq 1.3$) sinters prepared by means of optimized glycine-nitrate combustion and mechanical milling (Ref 1).

The data presented in Table 3 show that the porosity of sinters significantly affects their electrical conductivity. Since all studied sinters have comparable porosity, their conductivity values are also on a similar level. The sinter prepared using the powder obtained after calcinating the gel at 873 K exhibits the highest measured electrical conductivity at 1073 K, i.e., 88.4 S cm^{-1}. Taking into account the fact that the electrical conductivity of the coating material at IT-SOFC operating temperatures of 923-1123 K should be above 50 S cm^{-1}, all materials listed in Table 3 can serve this purpose; the $Cu_{1.3}Mn_{1.7}O_4$ sinter prepared using powder obtained after calcination at 873 K is especially suitable. Consequently, the authors propose this material as a candidate for ferritic stainless steel interconnects for IT-SOFC applications.

4. Conclusions

1. EDTA gel processes combined with thermal treatment of gels in the temperature range of 673-973 K were used to obtain a number of nanometric powders of a manganese-copper spinel with the desired chemical and phase composition.
2. Phase composition analysis performed for powders obtained after calcinating the gel at temperatures below 973 K revealed the presence of a main spinel phase with the composition of $Cu_{1.5}Mn_{1.5}O_4$ and small amounts of Mn_2O_3, while above 973 K a small amount of Mn_3O_4 was also present in addition to the above-mentioned main phase.
3. XRD observations of the sinters obtained after thermally treating green bodies prepared using powders calcinated at temperatures of 673, 773, 873, and 973 K revealed a predominant amount of spinel as well as certain amounts of the Mn_3O_4 phase and—with the exception of the sinter obtained from the powder calcinated at 673 K—CuO.
4. In the case of all investigated sinters, a change in the mechanism of electrical conduction in the temperature range of 400-430 K and a twofold increase in the activation energy of electrical conductivity above 430 K—to a level of 0.56 eV—are observed. Due to the comparable porosity of all sinter samples (ca. 12%), the differences in their electrical conductivity values were not significant. The highest measured electrical conductivity at 1073 K, i.e., 88.4 S cm^{-1}, was observed for the sinter prepared from the powder obtained after calcinating the gel at 873 K. This sinter can be considered a potentially suitable material for protective-conducting coatings on metallic interconnects based on ferritic stainless steel and intended for application in IT-SOFCs.

References

1. N. Hosseini, F. Karimazadeh, M.H. Abbasi, and G.M. Choi, Microstructural Characterization and Electrical Conductivity of $Cu_xMn_{3-x}O_4$ ($0.9 \leq x \leq 1.3$) Spinels Produced by Optimized Glycine-Nitrate Combustion and Mechanical Milling Processes, *Ceram. Int.*, 2014, **40**, p 12219–12226
2. A. Petric and H. Ling, Electrical Conductivity and Thermal Expansion of Elevated Temperatures, *J. Am. Ceram. Soc.*, 2006, **90**, p 1515–1520
3. J.B. Goodenough, *Magnetism and Chemical Bond*, Interscience Publishers Inc. and John-Wiley Inc., New York, 1963
4. N. Hosseini, M.H. Abbasi, F. Karimzadeh, and G.M. Choi, Development of $Cu_{1.3}Mn_{1.7}O_4$ Spinel Coating on Ferritic Stainless Steel for Solid Oxide Fuel Cell Interconnects, *J. Power Sources*, 2015, **273**, p 1073–1083
5. S. Molin, B. Kusz, M. Gazda, and P. Jasinski, Protective Coatings for Stainless Steel for SOFC Applications, *J. Solid State Electrochem.*, 2008, **13**, p 1695–1700
6. S. Molin, M. Chen, and P.V. Hendriksen, Oxidation Study of Coated Crofer 22 APU Steel in Dry Oxygen, *J. Power Sources*, 2013, **251**, p 488–495
7. D. Szymczewska, S. Molin, V. Venkatachalam, M. Chen, P. Jasinski, and P.V. Hendriksen, Assesment of $(Mn, Co)_3O_4$ Powders for Possible Coating Material for SOFC/SOEC Interconnects, *IOP Conf. Ser. Mater. Sci. Eng.*, 2015, **104**, p 1–9
8. S. Molin, P. Jasinski, L. Mikkelsen, W. Zhang, M. Chen, and P.V. Hendriksen, Low Temperature Processed $MnCo_2O_4$ and $MnCo_{1.8}Fe_{0.2}O_4$ as Effective Protective Coatings for Solid Oxide Fuel Cell Interconnects at 750 °C, *J. Power Sources*, 2016, **336**, p 408–418
9. T. Brylewski, A. Kruk, M. Bobruk, A. Adamczyk, J. Partyka, and P. Rutkowski, Structure and Electrical Properties of Cu-Doped Mn-Co-O Spinel Prepared Via Soft Chemistry and Its Application in Intermediate-Temperature Solid Oxide Fuel Cell Interconnects, *J. Power Sources*, 2016, **333**, p 145–155
10. M.J. Garcia-Vargas, M. Zahid, F. Tietz, and A. Aslnides, Use of SOFC Metallic Interconnect Coated with Spinel Protective Layers Using the APS Technology, *ECS Trans.*, 2007, **7**, p 2399–2405
11. Y. Xu, Z. Wen, S. Wang, and T. Wen, Cu Doped Mn-Co Spinel Protective Coating on Ferritic Stainless Steels for SOFC Interconnect Applications, *Solid State Ionics*, 2011, **192**, p 561–564
12. A. Kruk, M. Stygar, and T. Brylewski, Mn-Co Spinel Protective-Conductive Coatings on AL453 Ferritic Stainless Steel for IT-SOFC Interconnect Application, *J. Solid State Electrochem.*, 2013, **17**, p 993–1003
13. B.-K. Park, J.-W. Lee, S.-B. Lee, T.-H. Lim, S.-J. Park, Ch.-O. Park, and R.-H. Song, Cu- and Ni-Doped $Mn_{1.5}Co_{1.5}O_4$ Spinel Coatings on Metallic Interconnects for Solid Oxide Fuel Cell, *Int. J. Hydrogen Energy*, 2013, **38**, p 12043–12050
14. S. Joshi, C. Silva, P. Wang, Y. Mozharivskyj, and A. Petric, Copper-Magnesium-Manganese Spinel Coatings for Solid Oxide Fuel Cell Interconnects, *J. Electrochem. Soc.*, 2014, **161**, p F233–F238
15. Y. Wang, *Structure and Electrical Conductivity of Mn-Based Spinels Used as Solid Oxide Fuel Cell Interconnect Coatings*, Master of Applied Science, McMaster University (Materials Science and Engineering), Hamilton, Ontario, 2013
16. S.I. Hussein, A.S. Elkady, M.M. Rashad, A.G. Matafa, and R.M. Megahid, Structural and Magnetic Properties of Magnesium Ferrite Nanoparticles Prepared Via EDTA-Based Sol-Gel Reaction, *J. Magn. Magn. Mater.*, 2015, **379**, p 9–15
17. T. Brylewski, W. Kucza, A. Adamczyk, A. Kruk, M. Stygar, M. Bobruk, and J. Dąbrowa, Microstructure and Electrial Properties of $Mn_{1+x}Co_{2-x}O_4$ ($0 \leq x \leq 1.5$) Spinels Synthesized Using EDTA-Gel Processes, *Ceram. Int.*, 2014, **40**, p 13873–13882
18. M. Kakihana, Sol-Gel Preparation of High Temperature Superconducting Oxides, *J. Sol-Gel. Sci. Technol.*, 1996, **6**, p 7–55
19. L.G Sillèn and A.E. Martell, *Stability Constants of Metal-Ion Complexes*, Spec. Publ. Nos. 17 and 25 (Chemical Society, London, 1964 and 1972)
20. P. Scherrer, *Göttinger Nachrichten Gesell*, 1918, **2**, p 98
21. S.T. Aruna, M. Muthuraman, and K.C. Patil, Combustion Synthesis and Properties of Strontium Lanthanum Manganites $La_{1-x}Sr_xMnO_3$ ($0 \leq x \leq 0.3$), *J. Mater. Chem.*, 1997, **7**, p 2499–2503
22. G.H. Jonker and J.H. Van Santen, Magnetic Compounds with Perovskite Structure III. Ferromagnetic Compounds of Cobalt, *Physica*, 1953, **19**, p 120–130
23. A.P.B. Sinha, N.R. Sanjana, and A.B. Biswas, On the Structure of Some Manganites, *Acta Crystallogr.*, 1957, **10**, p 439–440
24. M.H. Cohen and J. Jortner, Effective Medium Theory for the Hall Effect in Disordered Materials, *Phys. Rev. Lett.*, 1973, **30**, p 696–698